









Article

Transforming Conventional Construction Binders and Grouts into High-Performance Nanocarbon Binders and Grouts for Today's Constructions

Herda Yati Binti Katman ^{1,*}, Wong Jee Khai ¹, Mehmet Serkan Kirgiz ^{2,*}, Moncef L. Nehdi ³, Omrane Benjeddou ⁴, Blessen Skariah Thomas ⁵, Styliani Papatzani ⁶, Kishor Rambhad ⁷, Manoj A. Kumbhalkar ⁸ and Arash Karimipour ⁹

- ¹ Institute of Energy Infrastructure, Universiti Tenaga Nasional, Putrajaya Campus, Jalan IKRAM-UNITEN, Kajang 43000, Malaysia; wongjk@uniten.edu.my
- ² Department of Architecture, Faculty of Engineering and Natural Sciences, İstanbul Sabahattin Zaim University, İstanbul 34303, Turkey
- ³ Department of Civil Engineering, Faculty of Engineering, McMaster University, Hamilton, ON L8S 4M6, Canada; nehdim@mcmaster.ca
- ⁴ Civil Engineering Department, College of Engineering, Prince Sattam bin Abdulaziz University, Alkharj 16273, Saudi Arabia; benjeddou.omrane@gmail.com
- ⁵ Department of Civil Engineering, NIT, Calicut 673601, India; blessen@nitc.ac.in
- ⁶ Department of Surveying and Geoinformatics Engineering, School of Engineering, University of West Attica, 12243 Athens, Greece; spatzani@uniwa.gr
- ⁷ Department of Mechanical Engineering, St. John College of Engineering and Management, Palghar 401404, India; kishorsrambhad@gmail.com
- ⁸ Department of Mechanical Engineering, JSPM Narhe Technical Campus, Pune 411041, India; manoj.kumbhalkar@rediffmail.com
- ⁹ Department of Civil Engineering, University of Texas at El Paso (UTEP), El Paso, TX 79968, USA; akarimipour@miners.utep.edu
- * Correspondence: herda@uniten.edu.my (H.Y.B.K.); nakres42@yahoo.com (M.S.K.)



Citation: Katman, H.Y.B.; Khai, W.J.; Kirgiz, M.S.; Nehdi, M.L.; Benjeddou, O.; Thomas, B.S.; Papatzani, S.; Rambhad, K.; Kumbhalkar, M.A.; Karimipour, A. Transforming Conventional Construction Binders and Grouts into High-Performance Nanocarbon Binders and Grouts for Today's Constructions. *Buildings* **2022**, *12*, 1041. <https://doi.org/10.3390/buildings12071041>

Academic Editors: Ahmed Senouci and Abdelhafid Khelidj

Received: 27 May 2022

Accepted: 4 July 2022

Published: 19 July 2022

Publisher's Note: MDPI stays neutral with regard to jurisdictional claims in published maps and institutional affiliations.



Copyright: © 2022 by the authors. Licensee MDPI, Basel, Switzerland. This article is an open access article distributed under the terms and conditions of the Creative Commons Attribution (CC BY) license (<https://creativecommons.org/licenses/by/4.0/>).

Abstract: The transformation of conventional binder and grout into high-performance nanocarbon binder and grout was evaluated in this investigation. The high-performance nanocarbon grout consisted of grey cement, white cement, lime, gypsum, sand, water, and graphite nanoplatelet (GNP), while conventional mortar is prepared with water, binder, and fine aggregate. The investigated properties included unconfined compressive strength (UCS), bending strength, ultrasound pulse analysis (UPA), and Schmidt surface hardness. The results indicated that the inclusion of nanocarbon led to an increase in the initial and long-term strengths by 14% and 23%, respectively. The same trend was observed in the nanocarbon binder mortars with white cement, lime, and gypsum in terms of the UCS, bending strength, UPA, and Schmidt surface hardness. The incorporation of nanocarbon into ordinary cement produced a high-performance nanocarbon binder mortar, which increased the strength to 42.5 N, in comparison to the 32.5 N of the ordinary cement, at 28 days.

Keywords: nanocarbon; conventional binder mortar; high-performance nanocarbon binder mortar; non-destructive testing; mechanical properties

1. Introduction

Graphitic carbon is an abundant material that can be produced in either a natural or artificial way. Carbon-based nanomaterials are synthesized from high-purity graphite. Artificial graphite-based carbon nanomaterial manufacturing depends on the modified Hummers (MH) method, which is a chemical oxidation process. The graphite nanoparticle (GNP) has a lamination depth of 1.1 nanometers, a multilayer interval of 0.85 nanometers, and a depolarization ratio of 0.77 [1]. The inclusion of GNP in traditional cement composites has been investigated by many researchers [2–4]. In one study, the presence of GNP

triggered both compression strength and bending strength in cement-based materials [5]. Microstructural analyses have suggested that the GNPs act as nucleation sites, thus enhancing the release of calcite and the formation of calcium silicates. This will reduce the extension of internal microcracks and improve the field among the cement paste and gravel pile [4,6,7]. Various construction materials have used GNP as an addition in the production of self-consolidating cementitious systems [8], concrete with E-waste plastic coarse aggregates [9], geopolymers [10], electrically conductive cementitious composites [11], concrete incorporating nanographite by-products (ING) [12], cement reinforcement [13], and high-volume fly ash concrete containing graphene nanoplatelets [14]. The presence of GNP results in an improvement in both the microstructural and mechanical properties. A research and development effort [8] showed that the blending of 0.05% GNP by mass of cement led to a 57% increase in compressive strength and a 48% increase in flexural moment.

Ahmad et al. [10] densified cementitious composite by adding different proportions of GNP. The addition of 5% GNP to the cementitious composite enhanced the hardened density and the compression, tensile, and flexural strength by 11%, 38%, 31%, and 44%, respectively. In addition, the 5% GNP reduced the sorptivity and water absorption by 32.2% and 73.9%, respectively, in the cementitious composite. It also increased the ultrasound pulse quantity by 7.5% [10]. In 2021, Dong et al. [12] compared the effects of the addition of 1–5% GNP and ING on a number of concrete properties. They revealed that the ING was more effective in developing concrete conductivity than the GNP, because 1% ING decreased electrical resistivity by 70%; the GNP reduced electrical resistivity by only 11% at the same concentration [12]. Sun et al. [11] examined the effect of graphite and slag on the electrical and mechanical properties of cementitious composite. They found that the optimized content of slag and graphite developed balanced electrical and mechanical properties in the cementitious composites [11].

Chougan et al. [15] studied different dosages of GNP ranging from 0.1% to 1%, by weight of geopolymer, in a 3D-printed multi-binder geopolymer composite. Their results indicated that the flexural moment increased by 89% and 46% in the 3D-printed geopolymer with 1% GNP when compared to the same 3D-printed and casted geopolymers without any GNP. The compressive strength increased by 28% and 12% in the 3D-printed geopolymer with 1% GNP [15]. Another study carried out by Chougan et al. [16] determined the rheological behavior, density, mechanical properties, permeability, damping ratio, and electrical and thermal conductivity of high-performance cementitious nanocomposites containing GNP. The results of their work showed that after 28 days of water curing, the GNP provided increased density up to 16% and mechanical properties up to 30%, as well as a remarkable reduction in permeability for all high-performance cementitious nanocomposites. Moreover, the lowest content (0.01% GNP by weight of cement) showed the highest increase in the damping ratio and electrical and thermal conductivity—68%, 30%, and 55%, respectively—in cementitious nanocomposites [16].

Alatawna et al. [17] reported results related to the impact of GNP, carbon nanotubes (CNTs), graphene oxide (GO), and functionalized carbon nanotubes (f-CNTs) on the workability and strength of a cementitious nanocomposite. Between the four evaluated graphitic systems, 0.025% GO performed best as a nanoreinforcing addition, offering an increase of 60% in flexural moment and 30% in compressive strength. The most important difference between these works and the current manuscript is that the abovementioned works aimed to develop cement-based materials, including by-products, through the addition of GNP. The present study aimed to develop conventional construction binders that are currently used in the construction sector, e.g., cement, white cement, lime, and gypsum, instead. The main novelty of the current research is reminiscent of the legendary findings of the English inventor Sir Henry Bessemer with respect to steel manufacturing. In the late 1800s, he managed to reduce the cost of steel making and revolutionize structural engineering by blowing air through molten pig iron to remove impurities, therefore reducing the carbon content in steel manufacturing to soften construction steel. In this study, conventional con-

struction binders and construction binder-based materials were hardened with nanocarbon particles, such as GNPs.

In addition, the manufacturing industry is facing many problems, including the availability of natural raw materials and the increase in energy consumption and other expenses. High energy consumption has led to an increase in the emission of carbon dioxide into the atmosphere, which is associated with climate change [18]. Therefore, a reduction in the use of natural resources, together with the reuse and recycling of materials, may help to alleviate this problem. With the recycling and reusing of materials, the need for landfill space and virgin raw materials can be minimized. The efficient use of materials is key to a sustainable future, given that significant amounts of materials are consumed by the construction industry. Cement-based materials that are used in construction possess good compression properties, but they are generally weak in tension and less ductile than other metallic materials. Nanomaterials can be added to cementitious composites to improve their performance [19–22]. Therefore, the current study examined the impact of blending nanocarbon on a number of properties of grout containing different types of binder. The binder materials used were Portland cement, white cement, gypsum, or lime. Various destructive and non-destructive mechanical tests were performed, including compressive strength, bending strength, Schmidt surface hardness, and ultrasound pulse analysis. The correlations between the various properties were also determined. The most important innovation provided by this work was that a normal binder with a compressive strength of 32.5 MPa was transformed into a normal binder with a compressive strength of 42.5 MPa at 28 days just by adding nanocarbon and without increasing the cement content, which would also cause an increase in the carbon footprint of the formulation. Therefore, a sustainable formulation is offered with significant strength advantages.

2. Materials and Techniques

2.1. Materials

This research utilized standard cement, which exhibited a compressive strength of 32.5 MPa at the 28th day, as per BS EN 197-1:2011 [23]. The white cement used had the following characteristics: a Blaine fineness of 395 m²/kg, initial setting of 100 min, unit volume mass of 3100 kg/m³, compressive strength of 32.5 MPa at the 28th day, and bulk density of 1100 kg/m³ [2]. The properties of class E lime were 20% silica + alumina + iron oxide, 50% calcium + magnesium oxide, 25% insoluble residue, and 5% carbon dioxide; 5% residue on 300 µm; a compressive strength of 1 MPa at the 14th day; a compressive strength of 1.75 MPa at the 28th day; Le Chatelier expansion 10 mm; and a pH of 11.3 [2]. The gypsum used was calcium sulfate dihydrate (CaSO₄·2H₂O), which had a specific gravity of 2300 kg/m³ and a hardness of 2 Mohs according to ASTM C28/C 28-10 [24]. The sand used was siliceous-based fine gravel with a size below 2 mm. The water absorption, compacted unit volume mass, and pH were 0.9%, 2430 kg/m³, and 8.2, respectively. The GNP used consisted of 99.5% pure carbon with a particle radius size below 50 nm [2].

2.2. Methods

2.2.1. Design of Mixture

A comprehensive laboratory testing program was conducted to measure the effect of the same fraction of GNP on the properties of various binders. Graphite nanoparticle (GNP) was added to the following conventional mortars: Portland cement mortar; white mortar; gypsum mortar; and lime mortar. These conventional mortars with the addition of GNP are called advanced nanotechnological mortars. Tables 1 and 2 list the approximate mixture proportions for both conventional and advanced nanotechnological mortars.

Table 1. Mixture proportions (kg/m^3) of conventional mortars.

Type of Conventional Mortar	Mixture Proportion (kg/m^3)						
	Conventional Binder				Type of Supplement	Type of Mortar Material	
	CEM I 32.5N Cement	White Cement	Gypsum	Lime	GNP	Sand	Water
Control Portland cement mortar	586	0	0	0	0	1758	293
White cement mortar	0	586	0	0	0	1758	293
Gypsum mortar	0	0	586	0	0	1758	293
Lime mortar	0	0	0	586	0	1758	293

Table 2. Mixture proportions (kg/m^3) of advanced nanotechnological mortars.

Type of Technological Nanocarbon Mortar	Technological Nanocarbon Binder					Types of Mortar Material	
	CEM I 32.5N Cement	White Cement	Gypsum	Lime	Graphite Nanoparticle (GNP)	Sand	Water
	Control Portland cement + GNP mortar	586	0	0	0	1.3	1758
White cement + GNP mortar	0	586	0	0	1.3	1758	293
Gypsum + GNP mortar	0	0	586	0	1.3	1758	293
Lime + GNP mortar	0	0	0	586	1.3	1758	293

Eight mortar mixes were prepared—four without GNP and four with GNP. The construction binding material consisted of either Portland binder, white binder, gypsum, or lime. The amount of GNP used in the mixes was $1.3 \text{ kg}/\text{m}^3$, which was equal to 0.22% of the weight of the construction binder (grey cement, white cement, gypsum, or lime) in the mortar (Table 2).

2.2.2. Casting and Preparation of Specimens

The binder, fine aggregate, and GNP (as per Tables 1 and 2) were first stirred in dry conditions for thirty seconds with a mixer at slow speed, followed by the addition of water. The fresh mortar was mixed again at slow speed for thirty seconds, then at a higher speed for another thirty seconds. The procedure was ceased for 15 s to scrape down the mortar specimen from the bowl side. Then, the mixer was rotated at a higher speed for another sixty seconds. The mixture was transferred to a prism formwork with a size of $50 \times 100 \times 200 \text{ mm}$. The hardening of the specimens in a curing cabinet lasted twenty-four hours; next, the formwork was removed, and all specimens were then water cured until testing and characterization.

2.2.3. Testing Aspect of Mortar Composite

The final features of the mortar composites which would allow for utilization by the end users were that the bending strength could not be under 0.1 MPa on the 28th day and 0.3 MPa on the 180th day and the compressive strength could not be under 3 MPa on the 28th day and 3.5 MPa on the 180th day in both the conventional binder mortar composite and high-performance nanocarbon binder mortar composite. The size of the specimens was kept constant at $50 \times 100 \times 200 \text{ mm}$.

2.2.4. Testing Regime

After demolding the specimens, solid binder mortars were tested to measure the compressive strength at day 28 and 180 according to BS EN 1015-11:2019 [25]. The compressive strengths of the binder mortar specimens were established with the ratio of pressure rising to $244.7 \pm 2.03 \text{ Kg}/\text{m}$. Five specimens were tested from each lot, and the findings were investigated using the descriptive statistical methods of standard deviation and arithmetic average. The mean of five compressive strength test results for the hardened binder mortar

was designated as a statistical description of compressive strength. Ultrasound pulse analysis (UPA) was performed using automatic pulse equipment on the binder mortar specimens according to rules of BS EN 12504-4:2021 [2,26] at 7 days. The transducers, lightly greased, were placed on both the longitudinal and transversal dimensions of prisms sized 50 mm × 100 mm × 200 mm. Five specimens were tested per mix. However, the pulse was established five times per specimen. The mean of the five UPA test results for the hardened binder mortar was designated as a statistical description of compressive strength.

To measure the surface hardness of the binder mortar specimen, a type N Schmidt hammer was used on the hardened binder mortar specimen according to BS EN 12504-4:2021 [2,26] at 7 days. Five specimens were tested for each mix. However, the Schmidt hammer was measured at least 10 times for each specimen.

The last measurement taken was the bending strength, which was performed on day 28 and 180. BS EN 1015-11:2019 [2,25] was followed to measure the bending strength. The bending strengths of the binder mortar specimens were established with the ratio of pressure rising to $2400 \pm 200 \text{ N s}^{-1}$. For each mix of binder mortar, five specimens were tested; the findings were evaluated according to the descriptive statistical values of standard deviation and arithmetic average. The mean quantity of five bending strength test results for the hardened binder mortar was designated as a statistical description of bending strength [2,25].

3. Findings and Arguments

3.1. Unconfined Strength of Compression (USC)

Figure 1 illustrates the USC results for mortar specimens with and without GNP. Adding GNP to conventional mortars increased the unconfined compressive strength for all curing periods. A water-to-binder ratio of 0.50 was kept constant for all mortar composites and was sufficient based on the amounts of the constituents in the mix.

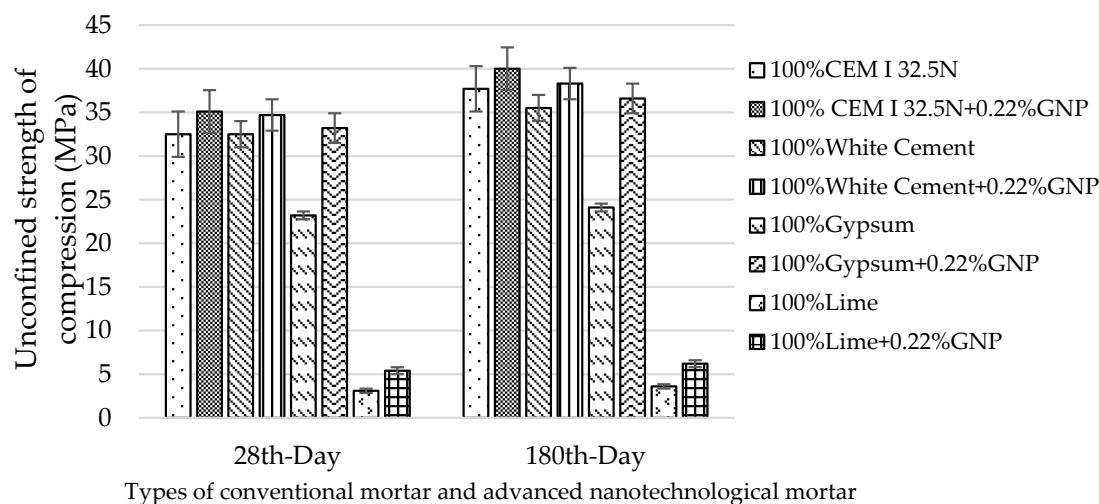


Figure 1. USC results for conventional and technological nanocarbon mortars after curing at 28 d and 180 d.

After 28 days, a maximum USC of 35.1 MPa for CEM type I 32.5 N + GNP mortar (Figure 1) was obtained. Thus, the addition of GNP proved to be a significant activator for Portland cement, white cement, gypsum, and lime binders. The USC of mortar containing GNP is related to the hydration of the cement and the activation reaction among the GNP and calcium hydroxide (CH), regardless of binder type. According to Meng and Khayat's results [23], ultra-high strength construction materials, including those supplemented with GNP, exhibited an ultra-high strength gain. The data indicate that there was a decrease in bulk density when using ash. This was due to the specific density of ash being lower than that of the sand it replaced. The USC results for the mortar composites with GNP

were slightly higher than for those without GNP at 28 d and 180 d (Figure 1). Due to the powerful effect of GNP, the calcium hydroxide was transformed to calcium carbonate hydroxide hydrate (CCH), and even at the later age (180 d), the determined USC for the mortars containing GNP was greater than that of the conventional mortars.

3.2. Mathematical Model for Predicting the Unconfined Strength of Compression

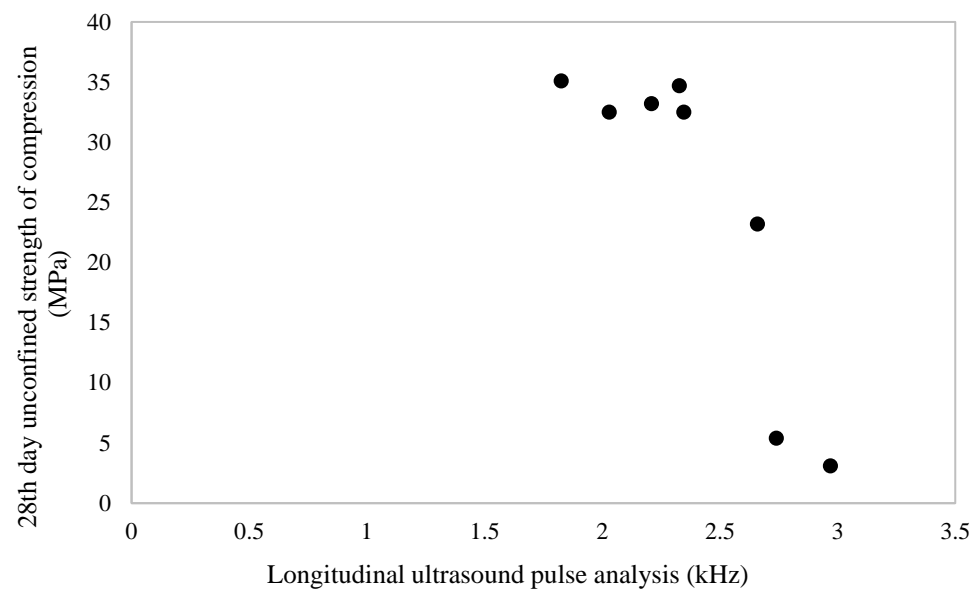
Popovics et al. showed that compressive strength is related to the components of cement-based materials [27]. The curve of calibration varies with material, and regression finding addresses the complicated features of mortar. The character of compaction and proper dispersion should be used to estimate the strength gain. The conclusions of these authors' research on regressions between the UPA and the strength of compression of binder material must be established, such as unit volume mass, Schmidt surface hardness, stiffness, etc. [28].

Recently, many works on the relationships between setting time and hardening utilizing ultrasound testing (UT) for cement and concrete materials have been published [29–31]. In these works, the compressive strengths of the samples are not specified; however, the suggested regression among compressive strength and ultrasound pulse analysis is a mathematical model of both power law and exponential functions in the calcium aluminate cement (CAC) mortar [32]. The authors point out that the suggested regression should be used only for cement-based materials with similar compositions.

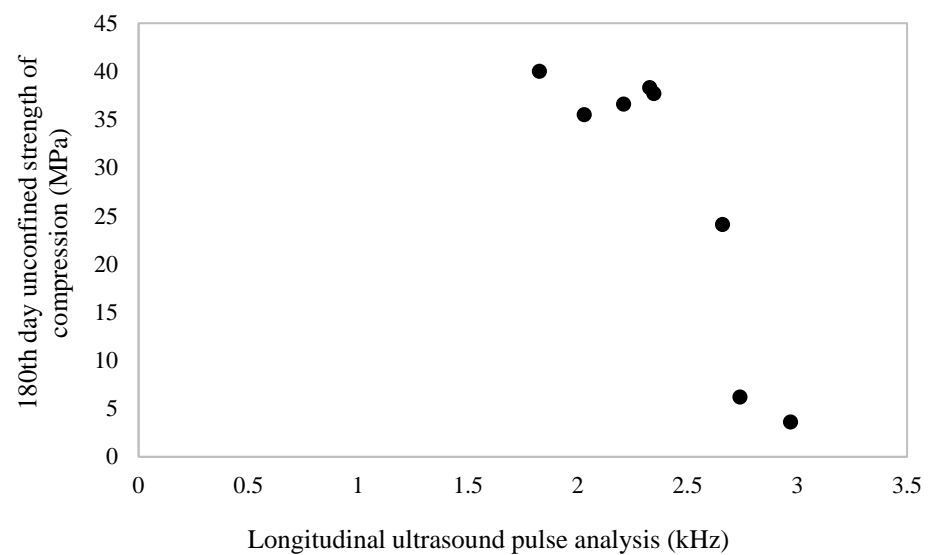
Recently, an exponential model for strength and pulse was proposed [33]. The models were developed one step further through a combined method using both UPA and its magnitude in estimating the strength of compression of cement-based materials. In the literature on strength estimation, there are a few challenges related to the possibility of establishing a regular correlation among the strength of compression and UPA for cement-based materials in terms of changes in the (i) mixture constituents, (ii) curing conditions, (iii) binder type, and (iv) various supplementary cementitious materials (SCM) added. Yet, various non-destructive testing (NDT) methods and estimation equations for strength have been utilized to examine the endurance and conformity of binder-based mortar composites. To investigate the compressive strength of mortar composites containing various binders, UPA is the NDT method used currently [34]. UPA is commonly utilized to establish material properties. It is also used to measure and estimate the dynamic elastic moduli and Poisson ratio of cement-based materials [35,36]. Thus, for each of the mortar composites, the relationship between the USC and UPA must be set; nevertheless, the complicated inner structure of the mortar composite may cause the data to be spread over a broad area [37].

Mohammed et al. [38] and Tsioulou et al. [39] suggested a correlation between the strength of compression and the UPA of cement-based materials using rubber additions. Rao et al. [35] suggested another correlation between the compressive strength and UPA of roller-compacted building material using ash in pavement practices. Furthermore, it is possible to use the UPA method to evaluate the density and porosity of hardened cement-based materials as well as to measure the uniformity of the material, detect cracks and honeycomb areas, and estimate the compressive strength [35]. A standard correlation among the UPA and USC of binder-based mortar composites is needed. Figure 2 presents a powerful correlation among the unconfined strength of compression and longitudinal UPA on the (a) 28th day and (b) 180th day.

The suggested math models for predicting the unconfined compressive strength from longitudinal UPA on the 28th day and 180th day are demonstrated in Equations (1) and (2), respectively, in Table 3.



(a)



(b)

Figure 2. Correlation among the unconfined strength of compression and longitudinal UPA on the (a) 28th day and (b) 180th day.

Table 3. Calibration equations for predicting unconfined strength of compression from longitudinal UPA.

Number	Calibration Equation	Correlation Coefficient (r^2)	Parameter
Equation (1)	$y = 4898.6x^6 - 68655x^5 + 398854x^4 - 1 \times 10^6x^3 + 2 \times 10^6x^2 - 2 \times 10^6x + 738241$	0.99	y represents unconfined strength of compression at 28 days and x is the longitudinal UPA at 7 days.
Equation (2)	$y = 3962.4x^6 - 55231x^5 + 319161x^4 - 978911x^3 + 2 \times 10^6x^2 - 2 \times 10^6x + 579862$	0.99	y represents unconfined strength of compression at 180 days and x is the longitudinal UPA at 7 days.

In light of this explanation, we expect that these equations can be used in practices such as the tracking of material conformity and the qualitative and quantitative evaluation of construction and detrimental effects, e.g., frosting and thawing, earthquake, and fire. Possibly, the equations could be found in practices regarding the conservation of existing buildings and cultural heritage. By rapidly measuring the material response non-destructively, the results of non-destructive measurement can be compared with materials that are not subjected to difficult conditions in terms of homogeneity, uniformity, and monitoring the deterioration of material properties with time. Figure 3 illustrates the powerful correlation among the unconfined strength of compression and transversal UPA on the (a) 28th day and (b) 180th day.

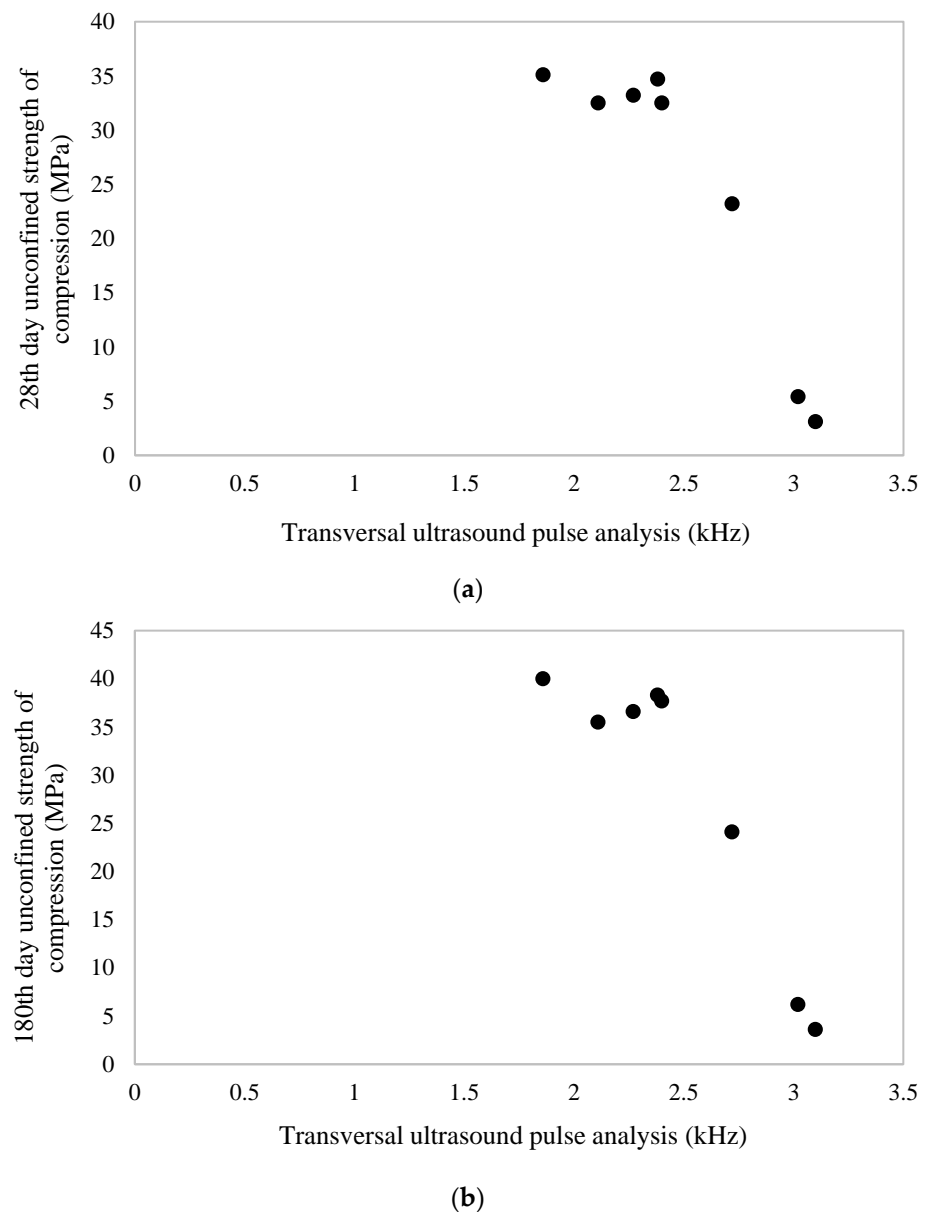


Figure 3. Powerful correlation among the unconfined strength of compression and transversal UPA on the (a) 28th day and (b) 180th day.

The suggested calibration equations for predicting the unconfined strength of compression from transversal UPA on the 28th day and 180th day are demonstrated in Equations (3) and (4), respectively, in Table 4.

Table 4. Calibration equations for predicting unconfined strength of compression strength from transversal UPA.

Number	Calibration Equation	Correlation Coefficient (r^2)	Parameter
Equation (3)	$y = -64.743x^6 + 1036.2x^5 - 6725.3x^4 + 22689x^3 - 42022x^2 + 40558x - 15916$	0.99	y represents unconfined strength of compression at 28 days and x is the transversal UPA at 7 days.
Equation (4)	$y = -638.05x^6 + 9610.7x^5 - 59778x^4 + 196474x^3 - 359867x^2 + 348283x - 139117$	0.99	y represents unconfined strength of compression at 180 days and x is the transversal UPA at 7 days.

Figure 4 presents the powerful correlation among the unconfined strength of compression and Schmidt surface hardness on the (a) 28th day and (b) 180th day. In the Schmidt hammer test, the outer firmness was established by number of rebounds when using the hammer of Schmidt. The hammer includes a steel spring that loads and slides throughout the bar; when allowed, it impacts with the help of a steel plunger on the outer surface of binder-based materials. The mass of steel shoots back from the steel plunger after impact. A linear scale on the Schmidt hammer measures the opening of the hammer's rebound from the steel plunger, and one can calculate the non-destructive strength of compression through the correlation graph of a standard [40]. Therefore, the Schmidt hammer test provides information regarding both surface hardness and estimated compressive strength gain for scientists, industrialists, contractors, and construction end users. Here, the Schmidt surface hardness of various binder mortars was utilized to investigate their compressive strength with the help of the given curve of correlation for Schmidt surface hardness.

A linear and exponential correlation has been shown between the compressive strength and Schmidt surface hardness of ultra-high performance fiber-reinforced concrete. Another research team suggested an exponential correlation among the compressive strength and Schmidt surface hardness of concrete supplemented with rubber [38,39]. In this study, polynomial relationships were developed for estimating the compressive strength of various binder mortar composites on the 28th and 180th day from Schmidt surface hardness.

The suggested calibration equations for predicting the unconfined strength of compression from Schmidt surface hardness on the 28th day and 180th day are demonstrated in Equations (5) and (6), respectively, in Table 5.

Table 5. Calibration equations for predicting unconfined strength of compression from longitudinal UPA.

Number	Calibration Equation	Correlation Coefficient (r^2)	Parameter
Equation (5)	$y = -0.0109x^6 + 0.876x^5 - 28.878x^4 + 499.09x^3 - 4760.6x^2 + 23730x - 48250$	1	y represents unconfined strength of compression at 28 days and x is the Schmidt surface hardness at 7 days.
Equation (6)	$y = -0.0077x^6 + 0.633x^5 - 21.425x^4 + 379.11x^3 - 36926x^2 + 18737x - 38688$	1	y represents unconfined strength of compression at 180 days and x is the Schmidt surface hardness at 7 days.

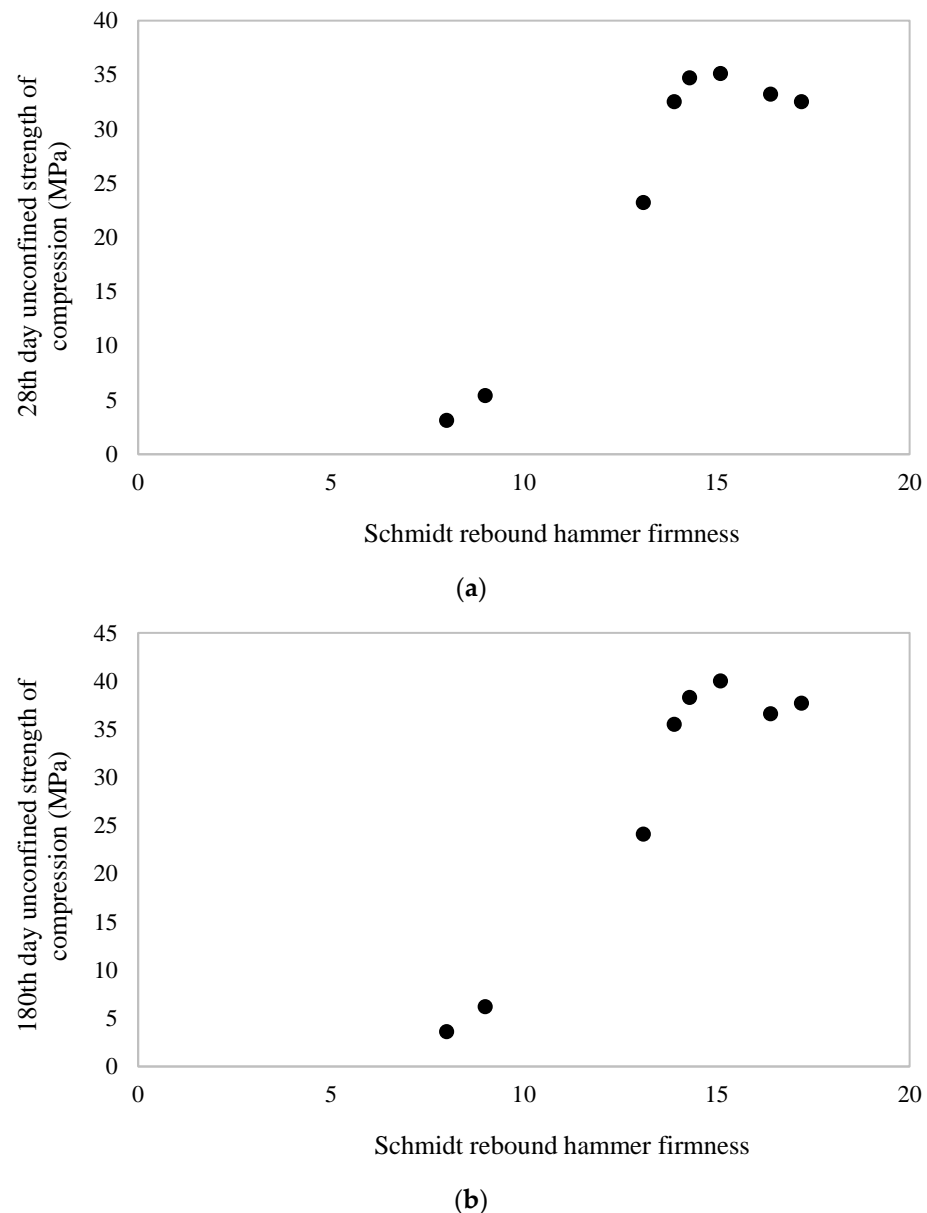


Figure 4. Powerful correlation among the unconfined strength of compression and Schmidt surface hardness on the (a) 28th day and (b) 180th day.

3.3. Ultrasound Pulse Analysis (UPA)

The continuous evaluation of the state of fresh mortar composite is required [40,41], and non-destructive methods are commonly utilized. The practice of ultrasound pulse analysis (UPA) in the quality control of cement-based material dates back to 1980 for ordinary cement types and blended cement types [42]. It can be measured in four different ways: longitudinal velocity measurement, transverse velocity measurement, and surface velocity measurement. In binder-based construction materials, the most commonly measured parameter is the longitudinal ultrasound pulse. The velocities of the transverse and outer-surface ultrasound pulses can be tested, and correlations among these UPA aspects and the physical and mechanical features of construction materials can be identified [27,43,44]. Figure 5 plots the UPA values in the longitudinal and transversal directions for the various mixes. Apart from the white cement mortar mix, the presence of GNP caused a reduction in UPA.

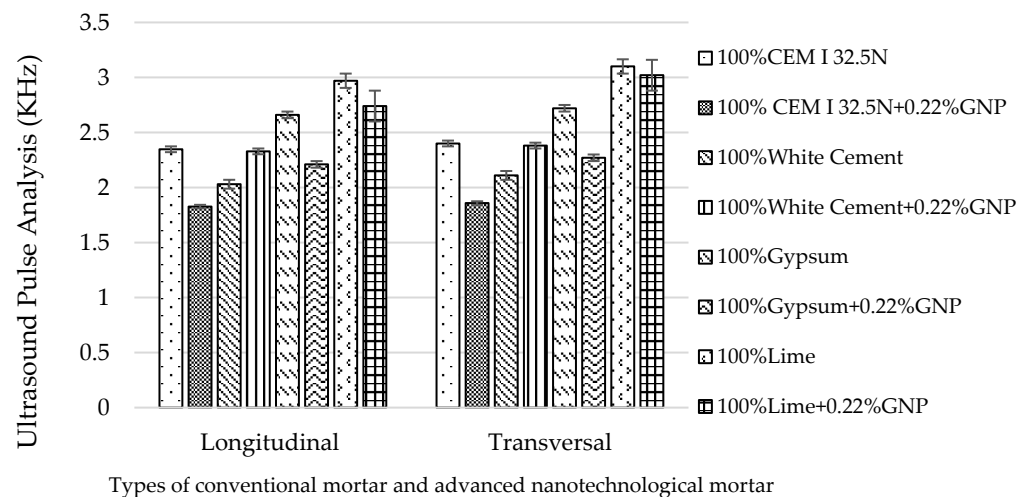


Figure 5. Changes in the UPA of various mortars and the binder type, binder percent, supplement type, and supplement percent.

It can be seen that the use of GNP in various mortars caused a decrease in both the longitudinal UPA and the transversal UPA. The use of GNP decreased the longitudinal UPA from 2.35 KHz, 2.03 KHz, 2.66 KHz, and 2.97 KHz to 1.83 KHz, 2.33 KHz, 2.21 KHz, and 2.74 KHz for the Portland cement mortar, white cement mortar, gypsum mortar, and lime mortar, respectively. Furthermore, the addition of GNP reduced the transversal UPA from 2.4 kHz, 2.11 kHz, 2.72 kHz, and 3.1 kHz to 1.86 kHz, 2.38 kHz, 2.27 kHz, and 3.02 kHz for the Portland cement mortar, white cement mortar, gypsum mortar, and lime mortar, respectively. This reduction in UPA with the addition of GNP could be related to the enrichment effect of the GNP on the constituents of the hydration product; a reduction in UPA means a reduction in strength and in hydration products, especially the calcium silicate hydrate. Since nanocarbon increases the compaction in mortar composites, which include Portland cement, white cement, gypsum, and lime, various strong regressions among compressive strength, bending strength, and UPA are also reported in the following subsection.

The classification of the quality of binder-based composites depends on the UPA value. If the UPA is more than 4 km/s, the binder-based composite has very good to excellent quality; if the UPA is between 3.5 and 4 km/s, the binder-based composite has favorable to very favorable quality and possibly some porosity; if the UPA is between 3 and 3.5 km/s, the quality of the binder-based composite is satisfactory, but a loss in integrity is suspected; if the UPA is under 3 (km/s), the quality of the binder-based composite is poor and a loss in integrity exists [45,46]. This quality assessment is a guideline for classifying binder-based composites using UPA test results. In addition to this classification, Himawan et al. [47] evaluated the quality of graphite material. Their results indicated that the graphite material showed frequency amplitudes between 2.4 and 3 km/s in the UPA test. According to the UPA classification above, the mortar composite containing cement was a very soft material with good quality.

3.4. Schmidt Surface Hardness

Figure 6 shows the change in the Schmidt surface hardness of the mortar composites as a function of 28d of water curing. The addition of GNP increased the Schmidt surface hardness from 17.2% to 15.1% for Portland cement mortar; 13.9% to 14.3% for white cement mortar; 13.1% to 16.4% for gypsum mortar; and 8% to 9% for lime mortar. This positive effect of the GNP is due to the generation of the hydration product and the reduction in pores related to the water in the mixture.

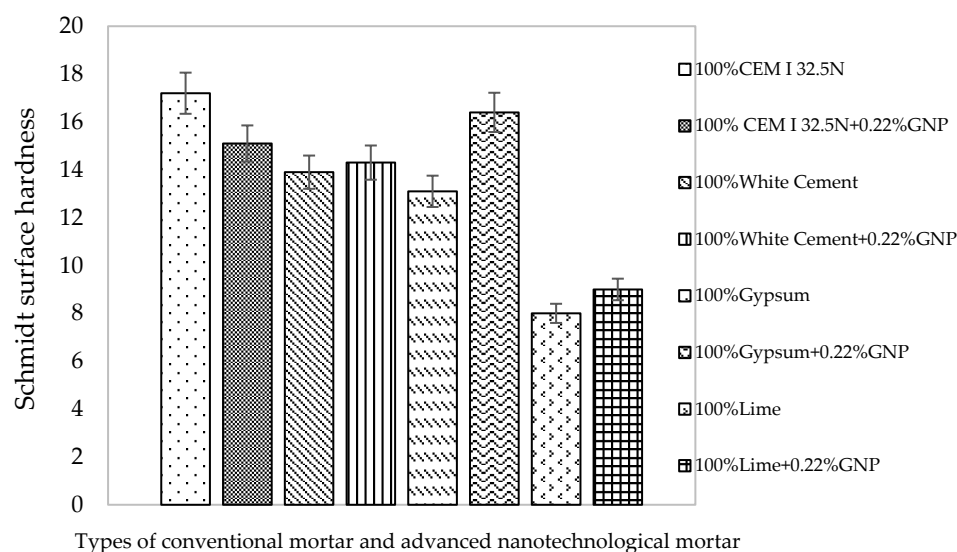


Figure 6. Changes in the Schmidt surface hardness of the various types of mortars and the binder type, binder percent, supplement type, and supplement percent.

This experiment consists of a sclerometer test, impact hammer, and rebound hammer and is a non-destructive method for testing binder-based composite materials. There is an approximately 45–50% experimental relation among Schmidt surface hardness and the unconfined strength of compression [48]. This correlation is related to aspects affecting the outer surface of cement-based materials; that is, the degree of saturation, carbonation, and coarse aggregate reaching the surface. Therefore, the Schmidt surface hardness test is helpful for determining the conformity and individual character of cement-based composite materials in construction.

In addition to UPA material classification, there is another quality assessment for the surface hardness of binder-based composites that depends on the results of the Schmidt rebound hammer test. When assessing surface hardness using the Schmidt rebound hammer, if the rebound number is more than 60, the composite is a very strong material; if the rebound number is between 50 and 60, the composite is a strong material; if the rebound number is between 40 and 50, the composite is a moderately strong material; if the rebound number is between 35 and 40, the composite is a weak material; if the rebound number is between 10 and 35, the composite is a very soft material [45,46]. According to the material classification with the Schmidt hammer test, the mortar composite was a very soft material with good quality as well. This result supports the classification of the mortar composites using UPA.

3.5. Bending Strength

Mortar has a highly complicated structure that not only responds to applied stresses but is also related to the interaction between its components. The inner structure of a mortar composite containing a broad range of aggregates differs from that of a bulk binder particle or supplementary particle, as this affects the morphology of the interfacial zone of transition (ITZ). The ITZ, in turn, significantly affects the firmness, bending strength, and capillarity in binder-based mortar composites with fine mortar sand, due to its lower density and delayed strength when compared to binder paste. Figure 7 shows the change in the bending strength of the mortar composites as a function of water curing.

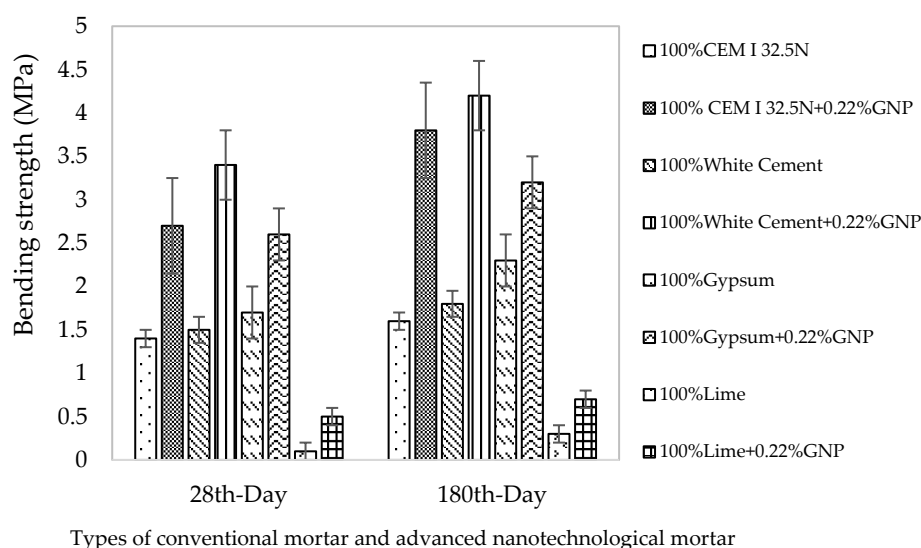


Figure 7. Changes in the bending strength of various types of mortars and the binder type, binder percent, supplement type, and supplement percent.

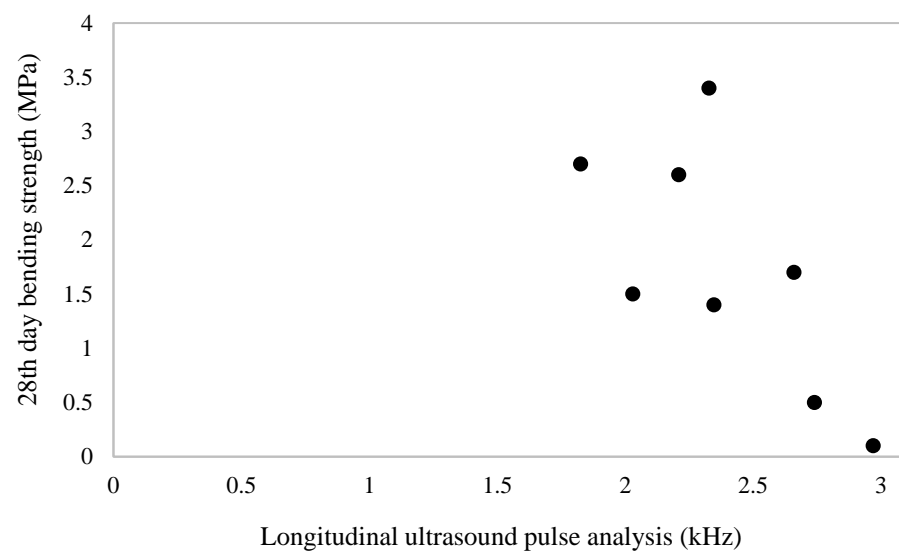
The addition of GNP increased the 28d bending strength from 1.4, 1.5, 1.7, and 0.1 MPa to 2.7, 3.4, 2.6, and 0.5 MPa for the Portland cement mortar, white cement mortar, gypsum mortar, and lime mortar, respectively. At 28 d, the addition of GNP to the mortar composite made of 100% CEM I 32.5N cement led to a 92% increase in the bending strength; beyond this increase, a remarkable hardness was also observed. The bending strength of the mortar composite containing white cement increased by up to 266.67% with the addition of GNP. The comparative increment in the bending strength of 100% gypsum and 100% lime mortar composites with GNP were recorded as 52.9% and 500%, respectively. Additionally, an increase similar to that of the 28d bending strength was also provided by the GNP supplement for the 180d bending strength of the mortar composites. A GNP concentration of 0.22% also increased the 180d bending strength from 1.6 MPa, 1.8 MPa, 2.3 MPa, and 0.3 MPa to 3.8 MPa, 4.2 MPa, 3.2 MPa, and 0.7 MPa for the Portland cement mortar, white cement mortar, gypsum mortar, and lime mortar, respectively. At 180 d, the addition of 0.22% GNP to the mortar composite made of 100% CEM I 32.5N cement led to an increase of 237.5% in the bending strength; similarly, a remarkable strength gain was also observed. The bending strength of the mortar composite containing white cement increased by up to 233.3% with the addition of 0.22% GNP. The comparative increment in the bending strength of the 100% gypsum and 100% lime mortar composites with 0.22% GNP were recorded as 39.1% and 233.3%, respectively.

To better understand the effect of 0.22% GNP on the bending strength of the mortar composites, a comparison between the results of 28 d bending strength and 180 d bending strength tests is presented here. The effect of the addition of 0.22% GNP on bending strength from 28 days to 180 days of water curing was measured as a 40.7% increment for the 100% CEM I 32.5N mortar composite, a 23.5% increment for the 100% white cement mortar composite, a 23% increase for the 100% gypsum mortar composite, and a 40% increase for the 100% CEM I 32.5N mortar composite. These increments are in line with other research in which GNP caused a higher bending strength in zirconium [7,45], ultra-high performance concrete [49], self-consolidating cementitious systems [8], concrete with E-waste plastic coarse aggregate [9], geopolymers [10], electrically conductive cementitious composites [11], concrete incorporating an iron-particle contained nanographite by-product [12], and other construction binder-based materials [13–17]. Additionally, the highest bending strength of the mortar composites was observed with the addition of 0.22% GNP, which is also in line with other existing results demonstrating better bending strength properties in high-performance cementitious composites with GNP addition [50]. Other authors evaluated the properties of an aluminum–magnesium–silica combined material modified through hybrid

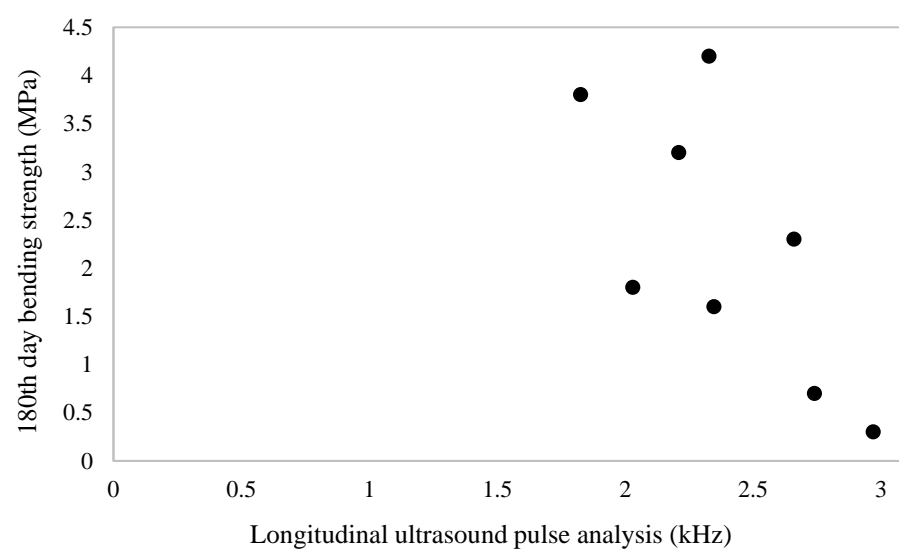
mixing and SiC powder [51]. Their results revealed that the stiffness of the composite rose by about 11% along with a rise in steel powder from four to eight percent, and the stress in the composite with 8% steel powder—compressive, bending, and splitting tensile—was greater than that of the composite modified with 8% SiC powder. These results can be attributed to the fact that SiC is tailored steel powder, which also contains carbon and could enhance the resiliency of the solid. Kurian et al. reported a new way to make nanocarbon and rubber [52]. They studied the mechanic, caloric, electronic, and electric properties and heat of the materials. They demonstrated that their nanocarbon rubber composite could protect resilient circuits and prevent increases in the temperature of sensors due to its thermal conductivity and stability as well as its non-deformability.

Mathematical Model for the Prediction of Bending Strength

Figure 8 shows the correlation between bending strength and the longitudinally measured UPA on (a) the 28th day and (b) the 180th day.



(a)



(b)

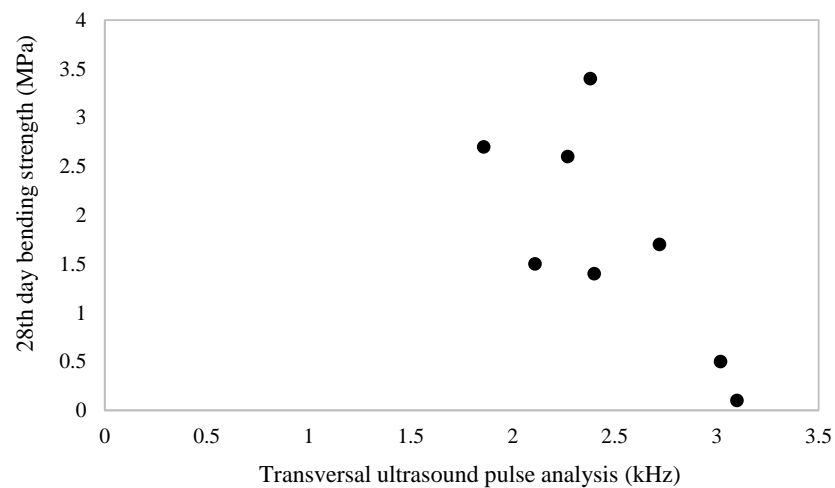
Figure 8. Strong regression relationship for the estimation of bending strength from the longitudinal UPA on (a) the 28th day and (b) the 180th day.

The suggested calibration equations for predicting the bending strength from the longitudinal UPA on the 28th day and 180th day are demonstrated in Equations (7) and (8), respectively, in Table 6.

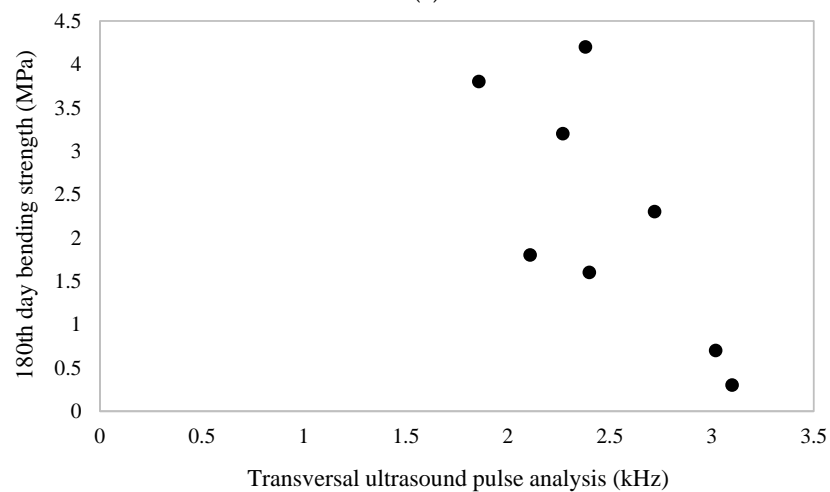
Table 6. Calibration equations for predicting bending strength from longitudinal UPA.

Number	Calibration Equation	Correlation Coefficient (r^2)	Parameter
Equation (7)	$y = 730.14x^6 - 10505x^5 + 62676x^4 - 198498x^3 + 35191x^2 - 331112x + 129156$	0.78	y represents bending strength at 28 days and x is the longitudinal UPA at 7 days.
Equation (8)	$y = 1043.1x^6 - 15002x^5 + 89467x^4 - 283212x^3 + 501847x^2 - 471938x + 183995$	0.76	y represents bending strength at 180 days and x is the longitudinal UPA at 7 days.

Figure 9 shows the correlation between bending strength and the transversal UPA on (a) the 28th day and (b) the 180th day.



(a)



(b)

Figure 9. Strong regression relationship for the estimation of bending strength from the transversal UPA on (a) the 28th day and (b) the 180th day.

The suggested calibration equations for predicting the bending strength from transversal UPA on the 28th day and 180th day are demonstrated in Equations (9) and (10), respectively, in Table 7.

Table 7. Calibration equations for predicting bending strength from transversal UPA.

Number	Calibration Equation	Correlation Coefficient (r^2)	Parameter
Equation (9)	$y = 322.71x^6 - 4932.1x^5 + 31219x^4 - 104732x^3 + 196363x^2 - 195049x + 80175$	0.79	y represents bending strength at 28 days and x is the transversal UPA at 7 days.
Equation (10)	$y = 463.83x^6 - 7072.9x^5 + 44670x^4 - 149640x^3 + 279801x^2 - 277393x + 113819$	0.77	y represents bending strength at 180 days and x is the transversal UPA at 7 days.

Figure 10 shows the powerful regression relationship between bending strength and Schmidt surface hardness on (a) the 28th day and (b) the 180th day.

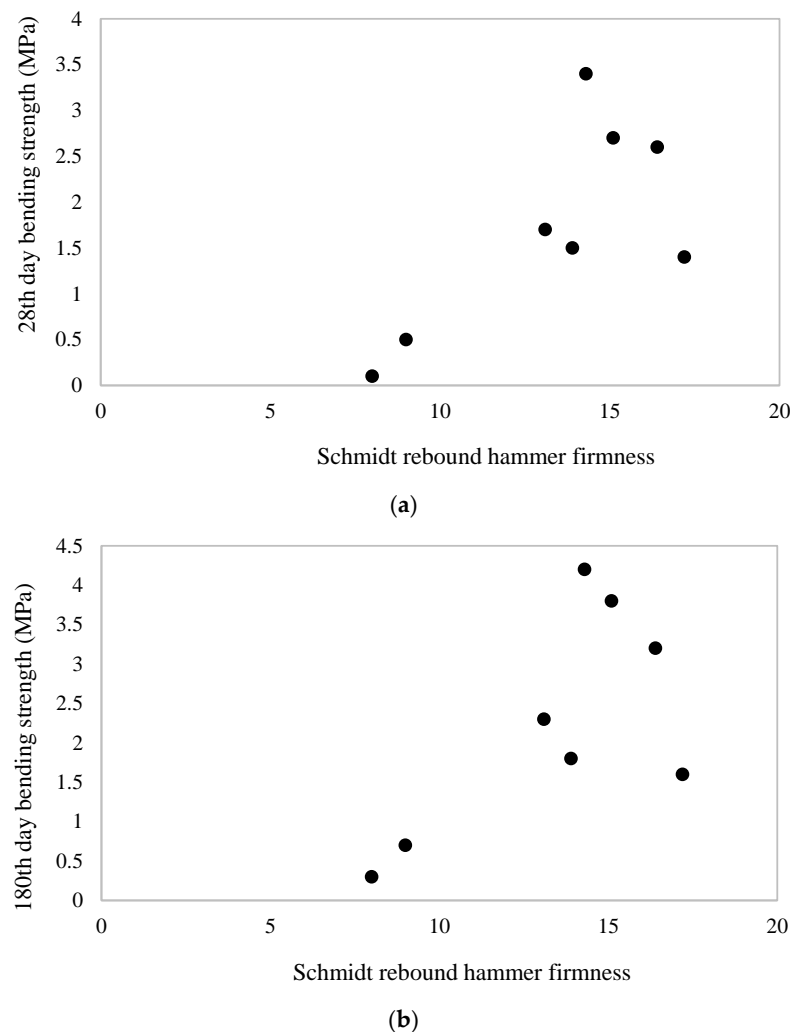


Figure 10. Strong regression relationship between bending strength and Schmidt surface hardness on (a) the 28th day and (b) the 180th day.

The suggested calibration equations for predicting the bending strength from Schmidt surface hardness on the 28th day and the 180th day are demonstrated in Equations (11) and (12), respectively, in Table 8.

Table 8. Calibration equations for predicting bending strength from Schmidt surface hardness.

Number	Calibration Equation	Correlation Coefficient (r^2)	Parameter
Equation (11)	$y = 0.0003x^6 - 0.0232x^5 + 0.7135x^4 - 11.446x^3 + 100.97x^2 - 464.49x + 870.86$	0.84	y represents bending strength at 28 days and x is Schmidt surface hardness at 7 days.
Equation (12)	$y = 0.0028x^6 - 0.2148x^5 + 6.8637x^4 - 115.11x^3 + 1067.4x^2 - 5183.9x + 10295$	0.86	y represents bending strength at 180 days and x is Schmidt surface hardness at 7 days.

4. Conclusions

The transformation of a conventional binder mortar into a high-performance nanocarbon binder mortar was investigated here. The following conclusions were drawn based on the results obtained:

- The use of GNP transformed conventional construction binders and grouts into high-performance nanocarbon binders and grouts by increasing the compression and bending strengths, which increased the strength to 42.5 N, in comparison to the 32.5 N of the ordinary cement, at 28 and 180 days;
- The high-performance nanocarbon binder mortar containing graphite nanoplatelet (GNP) exhibited the greatest UPA, Schmidt surface hardness, bending strength, and unconfined strength of compression;
- The initial and long-term strength of the high-performance nanocarbon gray binder mortar was increased by 14% and 23%, respectively, by the GNP. The nanocarbon binder mortars with white cement, lime, and gypsum showed same trend of initial and long-term strength gains in terms of UPA and Schmidt surface hardness. In addition, both the conventional construction binder mortar and high-performance nanocarbon gray binder mortar were classified as soft building materials by the UPA and Schmidt surface hardness guidelines given in the article;
- Many calibration equations were suggested to set a few powerful relationships between the USC and bending strength and the UPA and Schmidt surface hardness of conventional and high-performance nanocarbon binder mortars. The sixth relationship had the best correlation among these equations; therefore, it is the most suitable equation for estimating the USC and bending strength of mortars from their UPA and Schmidt surface hardness.
- GNP was identified as a beneficial supplement for today's construction binder-based mortars in terms of increasing their non-destructive and mechanical features. The present results and modelling of calibration equations could be applied as a benchmark to improve the performance of innovative infrastructure constructions, e.g., highways, dams, tall buildings, offshore structures, and public transportation road networks.

Author Contributions: Investigation, M.S.K.; writing—original draft preparation, M.S.K.; writing—review and editing, M.S.K., M.L.N., B.S.T., S.P., H.Y.B.K., O.B., W.J.K., K.R., M.A.K. and A.K.; supervision, M.S.K. All authors have read and agreed to the published version of the manuscript.

Funding: This research was funded by Universiti Tenaga Nasional grant number J510050002-IC-6 BOLDREFRESH2025-CENTRE OF EXCELLENCE. And The APC was funded by Universiti Tenaga Nasional.

Informed Consent Statement: Not applicable.

Data Availability Statement: No data, models, or code were generated or used during the study.

Conflicts of Interest: The authors declare no conflict of interest.

References

1. Kirgiz, M.S. Advancements in mechanical and physical properties for marble powder–cement composites strengthened by nanostructured graphite particles. *Mech. Mater.* **2016**, *92*, 223–234. [[CrossRef](#)]
2. Kirgiz, M.S. Green cement composite concept reinforced by graphite nano-engineered particle suspension for infrastructure renewal material. *Compos. Part B Eng.* **2018**, *154*, 423–429. [[CrossRef](#)]
3. Birenboim, M.; Nadv, R.; Alatawna, A.; Buzaglo, M.; Schahar, G.; Lee, J.; Kim, G.; Peled, A.; Regev, O. Reinforcement and workability aspects of graphene-oxide-reinforced cement nanocomposites. *Compos. Part B Eng.* **2019**, *161*, 68–76. [[CrossRef](#)]
4. Qureshi, T.S.; Panesar, D.K.; Sidhureddy, B.; Chen, A.; Wood, P.C. Nano-cement composite with graphene oxide produced from epigenetic graphite deposit. *Compos. Part B Eng.* **2019**, *159*, 248–258. [[CrossRef](#)]
5. Kirgiz, M.S.; de Sousa Galdino, A.G.; Kinuthia, J.; Khitab, A.; Hassan, M.I.U.; Khatib, J.; El Naggar, H.; Thomas, C.; Mirza, J.; Kenai, S.; et al. Synthesis, physico-mechanical properties, material processing, and math models of novel superior materials doped flake of carbon and colloid flake of carbon. *J. Mater. Res. Technol.* **2021**, *15*, 4993–5009. [[CrossRef](#)]
6. An, J.; Nam, B.H.; Alharbi, Y.; Cho, B.H.; Khawaji, M. Edge-oxidized graphene oxide (EOGO) in cement composites: Cement hydration and microstructure. *Compos. Part B Eng.* **2019**, *173*, 106795. [[CrossRef](#)]
7. Phrompet, C.; Sriwong, C.; Ruttanapun, C. Mechanical, dielectric, thermal and antibacterial properties of reduced graphene oxide (rGO)-nanosized C3AH6 cement nanocomposites for smart cement-based materials. *Compos. Part B Eng.* **2019**, *175*, 107128. [[CrossRef](#)]
8. Ullah, M.; Burhan, S.; Imtiaz, A.; Khushnood, R.A.; Erum Pervaiz, E.; Ahmed, W.; Ullah, A.; Qureshi, Z.A. Synthesis, characterization and application of graphene oxide in self consolidating cementitious systems. *Constr. Build. Mater.* **2021**, *296*, 123623. [[CrossRef](#)]
9. Ahmad, F.; Qureshi, M.I.; Ahmad, Z. Influence of nano graphite platelets on the behavior of concrete with E-waste plastic coarse aggregates. *Constr. Build. Mater.* **2022**, *316*, 125980. [[CrossRef](#)]
10. Jindal, B.B.; Sharma, R. The effect of nanomaterials on properties of geopolymers derived from industrial by-products: A state-of-the-art review. *Constr. Build. Mater.* **2020**, *252*, 119028. [[CrossRef](#)]
11. Sun, J.; Lin, S.; Zhang, G.; Sun, Y.; Zhang, J.; Chen, C.; Morsy, A.M.; Wang, X. The effect of graphite and slag on electrical and mechanical properties of electrically conductive cementitious composites. *Constr. Build. Mater.* **2021**, *281*, 122606. [[CrossRef](#)]
12. Dong, W.; Huang, Y.; Lehane, B.; Aslania, F.; Ma, G. Mechanical and electrical properties of concrete incorporating an iron-particle contained nano-graphite by-product. *Constr. Build. Mater.* **2021**, *281*, 121377. [[CrossRef](#)]
13. Sheikh, T.M.; Anwar, M.P.; Muthoosamy, K.; Jaganathan, J.; Chan, A.; Mohamed, A.A. The mechanics of carbon-based nanomaterials as cement reinforcement—A critical review. *Constr. Build. Mater.* **2021**, *303*, 124441. [[CrossRef](#)]
14. Adamu, M.; Trabanpruek, P.; Jongvivatsakul, P.; Likitlersuang, S.; Iwanami, M. Mechanical performance and optimization of high-volume fly ash concrete containing plastic wastes and graphene nanoplatelets using response surface methodology. *Constr. Build. Mater.* **2021**, *308*, 125085. [[CrossRef](#)]
15. Chougan, M.; Ghaffar, S.H.; Jahanzat, M.; Albar, A.; Mujaddedi, N.; Swash, R. The influence of nano-additives in strengthening mechanical performance of 3D printed multi-binder geopolymer composites. *Constr. Build. Mater.* **2020**, *250*, 118928. [[CrossRef](#)]
16. Chougan, M.; Marotta, E.; Lamastra, F.R.; Vivio, F.; Montesperelli, G.; Ianniruberto, U.; Ghaffar, S.H.; Al-kheetan, M.J.; Bianco, A. High performance cementitious nanocomposites: The effectiveness of nano-Graphite (nG). *Constr. Build. Mater.* **2020**, *259*, 119687. [[CrossRef](#)]
17. Alatawna, A.; Birenboim, M.; Nadv, R.; Buzaglo, M.; Peretz-Damari, S.; Peled, A.; Regev, O.; Sripada, R. The effect of compatibility and dimensionality of carbon nanofillers on cement composites. *Constr. Build. Mater.* **2020**, *232*, 117141. [[CrossRef](#)]
18. Khayati, G.R.; Ghasabe, H.M.; Karfarma, M.; Khayati, G.R.; Ghasabe, H.M.; Karfarma, M. A survey on the application of oxide nanoparticles for improving concrete processing. *Adv. Concr. Constr.* **2015**, *3*, 145. [[CrossRef](#)]
19. Alijani, M.; Bidgoli, M.R.; Alijani, M.; Bidgoli, M.R. Advances in Concrete Construction, Agglomerated SiO₂ nanoparticles reinforced-concrete foundations based on higher order shear deformation theory: Vibration analysis. *Adv. Concr. Constr.* **2018**, *6*, 585. [[CrossRef](#)]
20. Azmi, M.; Kolahchi, R.; Bidgoli, M.R.; Azmi, M.; Kolahchi, R.; Bidgoli, M.R. Dynamic analysis of concrete column reinforced with SiO₂ nanoparticles subjected to blast load. *Adv. Concr. Constr.* **2019**, *7*, 51. [[CrossRef](#)]
21. Tabatabaei, J.; Tabatabaei, J. The effect of TiO₂ nanoparticles in reduction of environmental pollution in concrete structures. *Adv. Concr. Constr.* **2019**, *7*, 127. [[CrossRef](#)]
22. Dorin, P.; Doina, P.; Simona, V.; Maria, P.; Stanca, C.; Codruta, S.; Marioara, M.; Raluca, I.; Razvan, E. Properties Evolution of Some Hydraulic Mortars Incorporating Graphene Oxides. *Buildings* **2022**, *12*, 864. [[CrossRef](#)]
23. BS EN 197-1:2011; Cement Composition, Specifications and Conformity Criteria for Common Cements. British Standards Institution: London, UK, 2019.

24. ASTM C 28/C 28-10(2020); Standard Specification of Gypsum Plasters. American Society of Testing and Materials: Conshohocken, PA, USA, 2020.
25. BS EN 1015-11:2019; Methods of Test for Mortar for Masonry—Determination of Flexural and Compressive Strength of Hardened Mortar. British Standards Institution: London, UK, 2019.
26. BS EN 12504-4:2021; Testing Concrete in Structures-Determination of Ultrasonic Pulse Velocity. British Standards Institution: London, UK, 2021.
27. Popovics, S.; Rose, J.L.; Popovics, J.S. The behaviour of ultrasonic pulses in concrete. *Cem. Concr. Res.* **1990**, *20*, 259–270. [[CrossRef](#)]
28. Krautkrämer, J.; Krautkrämer, H. *Ultrasonic Testing of Materials*; Springer: Berlin/Heidelberg, Germany, 1990; pp. 1–667; ISBN 978-3-662-10680-8. [[CrossRef](#)]
29. Valič, M.I. Hydration of cementitious materials by pulse echo USWR: Method, apparatus and application examples. *Cem. Concr. Res.* **2000**, *30*, 1633–1640. [[CrossRef](#)]
30. Smith, A.; Chotard, T.; Gimet-Breart, N.; Fargeot, D. Correlation between hydration mechanism and ultrasonic measurements in an aluminous cement: Effect of setting time and temperature on the early hydration. *J. Eur. Ceram. Soc.* **2002**, *22*, 1947–1958. [[CrossRef](#)]
31. Chotard, T.; Gimet-Breart, N.; Smith, A.; Fargeot, D.; Bonnet, J.P.; Gault, C. Application of ultrasonic testing to describe the hydration of calcium aluminate cement at the early age. *Cem. Concr. Res.* **2001**, *31*, 405–412. [[CrossRef](#)]
32. Mangabhai, R.J. *Calcium Aluminate Cements—The Influence of Superplasticising Admixtures on Ciment Fondu Mortars*; CRC Press: Boca Raton, FL, USA, 1990; pp. 1–14; ISBN 9780429078507.
33. Liang, M.T.; Wu, J. Theoretical elucidation on the empirical formulae for the ultrasonic testing method for concrete structures. *Cem. Concr. Res.* **2002**, *32*, 1763–1769. [[CrossRef](#)]
34. Latif Al-Mufti, R.; Fried, A.N. The early age non-destructive testing of concrete made with recycled concrete aggregate. *Constr. Build. Mater.* **2012**, *37*, 379–386. [[CrossRef](#)]
35. Rao, S.K.; Sravana, P.; Rao, T.C. Experimental studies in Ultrasonic Pulse Velocity of roller compacted concrete pavement containing fly ash and M-sand. *Int. J. Pavement Res. Technol.* **2016**, *9*, 289–301. [[CrossRef](#)]
36. Amini, K.; Jalalpour, M.; Delatte, N. Advancing concrete strength prediction using non-destructive testing: Development and verification of a generalizable model. *Constr. Build. Mater.* **2016**, *102*, 762–768. [[CrossRef](#)]
37. Bogas, J.A.; Gomes, M.G.; Gomes, A. Compressive strength evaluation of structural lightweight concrete by non-destructive ultrasonic pulse velocity method. *Ultrasonics* **2013**, *53*, 962–972. [[CrossRef](#)]
38. Mohammed, B.S.; Azmi, N.J.; Abdullahi, M. Evaluation of rubbercrete based on ultrasonic pulse velocity and rebound hammer tests. *Constr. Build. Mater.* **2011**, *25*, 1388–1397. [[CrossRef](#)]
39. Tsioulou, O.; Lampropoulos, A.; Paschalis, S. Combined Non-Destructive Testing (NDT) method for the evaluation of the mechanical characteristics of Ultra High Performance Fibre Reinforced Concrete (UHPFRC). *Constr. Build. Mater.* **2017**, *131*, 66–77. [[CrossRef](#)]
40. Chaix, J.F.; Garnier, V.; Corneloup, G. Concrete damage evolution analysis by backscattered ultrasonic waves. *NDT E Int.* **2003**, *36*, 461–469. [[CrossRef](#)]
41. Saad, M.; Abo-El-Enein, S.A.; Hanna, G.B.; Kotkata, M.F. Effect of silica fume on the phase composition and microstructure of thermally treated concrete. *Cem. Concr. Res.* **1996**, *26*, 1479–1484. [[CrossRef](#)]
42. Robson, T.D. *High-Alumina Cements and Concretes*; Wiley: London, UK; Contractors Record: New York, NY, USA, 1962; pp. 1–264.
43. Berthaud, Y. Damage measurements in concrete via an ultrasonic technique. Part I experiment. *Cem. Concr. Res.* **1991**, *21*, 73–82. [[CrossRef](#)]
44. Hwa, L.G.; Lee, G.W. Influence of water on the physical properties of calcium aluminate oxide glasses. *Mater. Chem. Phys.* **1999**, *58*, 191–194. [[CrossRef](#)]
45. Kirgiz, M.S. Determination of Physical and Mechanical Properties of Kırşehir Kaman Demirli Area Marbles. Master’s Thesis, Institute of Science and Technology, Gazi University, Ankara, Turkey, 2002.
46. Kirgiz, M.S. Usage of the Wastes of Marble and Brick Industries in Cement Manufacturing as Mineralogical Additive. Ph.D. Thesis, Institute of Science and Technology, Gazi University, Ankara, Turkey, 2007.
47. Himawan, R.; Lie, F.; Basoeki, P.D.; Haryanto, M. Applicability Study of Ultrasonic Flaw Detector for Nuclear Grade Graphite Examination. *J. Phys. Conf. Ser.* **2019**, *1198*, 022018. [[CrossRef](#)]
48. Fattahi, H. Applying soft computing methods to predict the uniaxial compressive strength of rocks from Schmidt hammer rebound values. *Comput. Geosci.* **2017**, *21*, 665–681. [[CrossRef](#)]
49. Meng, W.; Khayat, K.H. Mechanical properties of ultra-high-performance concrete enhanced with graphite nanoplatelets and carbon nanofibers. *Compos. Part B Eng.* **2016**, *107*, 113–122. [[CrossRef](#)]
50. Ahmad, F.; Jamal, A.; Iqbal, M.; Alqurashi, M.; Almoshaogeh, M.; Al-Ahmadi, H.M.; Hussein, E.E. Performance evaluation of cementitious composites incorporating nano graphite platelets as additive carbon material. *Materials* **2022**, *15*, 290. [[CrossRef](#)] [[PubMed](#)]
51. Alaneme, K.K.; Fajemisin, A.V.; Maledi, N.B. Development of aluminium-based composites reinforced with steel and graphite particles: Structural, mechanical and wear characterization. *J. Mater. Res. Technol.* **2019**, *8*, 670–682. [[CrossRef](#)]
52. Kurian, A.S.; Mohan, V.B.; Souril, H.; Leng, J.; Bhattacharyya, D. Multifunctional flexible and stretchable graphite-silicone rubber composites. *J. Mater. Res. Technol.* **2020**, *9*, 15621–15630. [[CrossRef](#)]